INTERNATIONAL JOURNAL FOR NUMERICAL METHODS IN FLUIDS
Int. J. Numer. Meth. Fluids **29**: 429–449 (1999)

A FINITE ELEMENT METHOD STUDY OF EULERIAN DROPLETS IMPINGEMENT MODELS

YVES BOURGAULT*, WAGDI G. HABASHI, JULIEN DOMPIERRE AND GUIDO S. BARUZZI

CFD Laboratory, Department of Mechanical Engineering, Concordia University, 1455 de Maisonneuve Blvd. W., ER-301, Montreal, Quebec, Canada H3G 1M8

SUMMARY

To compute droplet impingement on airfoils, an Eulerian model for air flows containing water droplets is proposed as an alternative to the traditional Lagrangian particle tracking approach. Appropriate boundary conditions are presented for the droplets equations, with a stability analysis of the solution near the airfoil surface. Several finite element formulations are proposed to solve the droplets equations, based on conservative and non-conservative forms and using different stabilization terms. Numerical results on single and multi-elements airfoils for droplets of mean volume diameter, as well as for a Langmuir distribution of diameters, are presented and validated against measured values. Copyright © 1999 John Wiley & Sons, Ltd.

KEY WORDS: in-flight icing; diphasic flow; droplet impingement; Eulerian droplets model; finite element

1. INTRODUCTION

In-flight icing has been, and still is, an active area of concern to aircraft and engine manufacturers, operators, pilots and regulators. Recent accidents indicate that the problem is not totally mastered. For example, ice accretion on aircraft lifting structures induces a loss of lift, a drag increase and a reduction of the stall angle. This performance deterioration, especially if sudden, has been identified in many cases as the cause of a crash. Another critical situation occurs if ice accumulates on engine inlets, and some of the ice is stripped by the incoming flow and ingested into the combustion chamber. If the ice chunks are large enough, their latent heat of sublimation can cause flameout.

The concerns are thus important enough for a lot of effort on experimental and analytical studies of the in-flight icing problem. Experiments in icing tunnels or behind icing tankers serve as a certification tool for new designs, as well as means to validate analytical models. Analytical models are research tools used to identify important physical processes behind the ice accretion. These analytical models also serve in the preliminary design phase of anti- and de-icing devices.

The numerical simulation of ice accretion and aerodynamic performance penalty has been traditionally based, as can be seen in the NASA Lewice [1] and ONERA codes [2], on inviscid

---

* Correspondence to: CFD Laboratory, Department of Mechanical Engineering, Concordia University, 1455 de Maisonneuve Blvd. W., ER-301, Montreal, Quebec, Canada H3G 1M8.

CCC 0271–2091/99/040429–21$17.50

Received August 1997
Revised January 1998

Panel or Euler plus boundary layer correction computations for the air flow and on Lagrangian particle tracking techniques for the droplets impingement. It is thought, however, that by solving the compressible Navier–Stokes equations, one can fully and more directly account for the influence of the viscous effects on the degradation of performance. If such a method is adopted, it would then be more natural to compute ice accretion on airfoils by an Eulerian model rather than the traditional Lagrangian particle tracking approach. Droplets velocity and volume fraction of water would have to be computed only at the nodes where the air flow variables are determined, and no particles would have to be tracked as they go through the mesh as in a Lagrangian approach. The net flux of water at the airfoil surface may also be recovered directly, while an averaging process would be needed with Lagrangian tracking after impacting particles have been detected. In 3D, such an averaging process is not evident to define and code, giving an additional advantage to the Eulerian approach.

While two-phase droplets flows have already been computed in an Eulerian manner in the past (see Crowe [3], Durst *et al.* [4], Hallman *et al.* [5] and references therein), to the authors' best knowledge, only one attempt has been made to use the Eulerian approach for icing droplets impingement [6]. In that study, although the objective was also to predict the flux of water on the leading edge of an airfoil, the technique was only applied to flows around a cylinder. A spatial marching scheme was used to solve the droplets equations, making complex configurations with recirculating flows difficult to handle. With such limitations, a major advantage of the Eulerian approach to droplets impingement was missed, namely the possibility of computing droplets impingement on multi-element airfoil configurations in an automatic way, without the tedious determination of launching areas for droplets to impact on each airfoil element, as in the Lagrangian approach.

It is therefore, the general purpose of the present paper to verify the mathematical well-posedness and the computational efficiency of an Eulerian model for impinging droplets. Not much emphasis will be put on the flow solver itself and simple laminar flows will be used in most test cases, as this paper concentrates on the Eulerian droplets model and avoids obscuring the results by the complexities of turbulent flow calculation. This, by no means, restricts the validity and the applicability of the method, as will be seen. In Section 2, the Eulerian droplets model is introduced. Boundary conditions with a stability analysis follow in Section 3. In Section 4, a finite element formulation is used to discretize the droplets equations. Appropriate stabilization terms needed to improve the numerical droplets solution are then compared. The recovery of the water collection efficiency in the Eulerian context is presented in Section 5. The viscous flow field computations are greatly enhanced via an efficient and novel anisotropic mesh adaptation procedure, and a brief discussion is given in Section 6. In Section 7, a comparison of numerical and experimental results is made, using a mean volume diameter (MVD), as well as a distribution of droplet diameters. Numerical results on multi-element airfoils and a comparison of large versus small droplets collection efficiencies are also presented.

2. EULERIAN DROPLETS MODEL

The classical compressible Navier–Stokes equations are the basis of the air flow computations, but an inviscid flow solver may be used as well, as the flow and droplets solvers are kept independent. No modification of the Navier–Stokes equations is needed even though droplets are present because the mass loading, i.e. the ratio of the bulk density[1] of the droplets over the

---

[1] The bulk density of a given phase is the mass of the phase in the mixture per unit volume of mixture.

bulk density of the air, is of the order of 10^{-3} in icing conditions. It is generally agreed that a loading smaller than 0.1 is well-modeled by a one-way coupling [3].

Using the Eulerian approach for the droplets, one tries to recover a volume fraction of water α and a velocity field $\mathbf{u}$. The variables $\alpha(x, t)$ and $\mathbf{u}(x, t)$ are mean values of the ratio of the volume occupied by water over the total volume of the fluid element and of the droplets velocity over the element, given a small fluid element around any specific location x in space at time t respectively The continuum hypothesis remains valid for the droplets phase as long as the fluid element contains enough droplets, say 10^4 for a fluctuation around the mean droplets volume fraction below 1% [3]. For typical icing conditions, i.e. for a MVD equal to 20 μm and a liquid water content (LWC) equal to 1 g m^{-3}, the length scale of the 1% fluctuation fluid element should be of the order of 1 cm. A smaller LWC would require a larger 1% fluctuation fluid element or a l cm fluid element should be associated with a droplets volume fraction fluctuation slightly larger than 1%.

A number of phenomena and forces may be considered while modeling air–droplets flows, but the following assumptions are sensible in in-flight icing situations:

- the droplets are spherical without any deformation or breaking;
- no droplets collision, coalescence or splashing;
- no heat and mass exchange between the droplets and the surrounding air;
- turbulence effects on the droplets can be neglected;
- the only forces acting on the droplets are due to air drag, gravity and buoyancy.

The first two assumptions rest on the fact that icing droplets are small (1–100 μm range) and the icing droplets flow should be considered dilute with a volume fraction around 10^{-6}. The gravity and buoyancy forces are kept in the model, even if they are three orders of magnitude lower than the drag force for typical flight applications. These forces could, however, be important for the simulation of de-icing fluid contamination by rain and snow during ground operation. Among the forces neglected on droplets, one may notice the effect induced by the unsteadiness of the flow around a droplet and the air pressure gradient in the vicinity of the droplet.

The continuity and momentum droplets equations are written, using non-dimensional variables, as

$$\frac{\partial}{\partial t} + \nabla \cdot (\alpha \mathbf{u}) = 0, \tag{1}$$

$$\frac{\partial \mathbf{u}}{\partial \mathrm{t}} + \mathbf{u} \cdot \nabla \mathbf{u} = \frac{C_{\mathrm{D}} Re_{\mathrm{d}}}{24K} (\mathbf{u}_{\mathrm{a}} - \mathbf{u}) + \left(1 - \frac{\rho_{\mathrm{a}}}{\rho}\right) \frac{1}{Fr^2} \mathbf{g}, \tag{2}$$

where α is the non-dimensionalized volume fraction of water; $\mathbf{u}$, the non-dimensionalized velocity of droplets, i.e. $\mathbf{u}/U_\infty$; $\mathbf{u}_{\mathrm{a}}$, the non-dimensionalized velocity of air; ρ, the density of water; ρ_{a}, the density of air; d is the droplets diameter; $Re_{\mathrm{d}} = (\rho d U_\infty |\mathbf{u}_{\mathrm{a}} - \mathbf{u}|)/\mu$ is the droplets Reynolds number; $K = \rho d^2 U_\infty / 18 L \mu$ is an inertia parameter; $C_{\mathrm{D}} = (24/Re_{\mathrm{d}})(1 + 0.015 Re_{\mathrm{d}}^{0.687})$ for $Re_{\mathrm{d}} \leq 1000$ and $C_{\mathrm{D}} = 0.4$ for $Re_{\mathrm{d}} > 1000$ is the drag coefficient for spherical droplets; $Fr = U_\infty / \sqrt{Lg}$ is the Froude number; U_∞, the speed of air at infinity; L is the characteristic length (typically the airfoil chord length); and μ, the dynamic viscosity of air.

The last term on the right-hand-side of the momentum equation accounts for gravity and buoyancy effects. The system (1) and (2) models the evolution of droplets having the same given diameter, usually chosen equal to the mean volume diameter (MVD) of the size distribution. The handling of multiple droplet sizes will be shown below by duplicating the number of equations solved, using the above system once for each class of diameters.

Obviously, Equation (2) is written in non-conservative form. The conservative form first derived using the principles of continuum mechanics would read instead as:

$$\frac{\partial \alpha \mathbf{u}}{\partial t} + \nabla \cdot (\alpha \mathbf{u} \otimes \mathbf{u}) = \frac{C_{\mathrm{D}} Re_{\mathrm{d}}}{24K} \alpha (\mathbf{u}_{\mathrm{a}} - \mathbf{u}) + \alpha \left(1 - \frac{\rho_{\mathrm{a}}}{\rho} \right) \frac{1}{Fr^2} \mathbf{g}. \tag{3}$$

The passage from (3) to (2) can be done in two steps, first by subtracting α times the droplet continuity equation from (3) and second, dividing the momentum equations then obtained by α, as α multiplies each of their terms.

One could question at first the validity of this latter division by α in the areas where the volume fraction of water is null. But, in these areas, a droplet velocity is recovered for non-existent droplets using Equation (2), and thus can take any value. Another interpretation comes from the fact that Equation (2) describes the evolution of the velocity at a given point instead of the droplets momentum, without considering the presence or the absence of droplets at this specific point. In other words, assuming one puts droplets at some point, their velocity would evolve according to Equation (2). Moreover, Equation (3) being satisfied provided Equation (2) is, although the reverse is not necessarily true, the latter equation puts more constraint on the droplets velocity. It is thus expected, and has been observed, that the use of the non-conservative form gives a more efficient code in terms of convergence behavior of the non-linear iterative solver, especially if the dependent variable is the droplets velocity instead of momentum.

Another point of concern with the non-conservative form (2) is the presence of droplets solution discontinuities and the appropriate description of their time evolution. For icing computations, the solution is smooth everywhere except near the contact discontinuity between the 'non-shadowed and shadowed area' besides the suction surface of the airfoil. The airfoil then becomes a screen for incoming droplets, defining what could be called a shadowed area behind the airfoil. In this shadowed area, the characteristics associated with the droplets velocity field generally meet the airfoil at some point whenever they are followed upstream (Figure 1). Thus, the droplets are removed or washed out from this shadowed area on the pressure surface and the volume fraction should be null in this region. Just the opposite, the droplets characteristics in the non-shadowed area should meet the outer domain boundary while followed upstream. The solution then presents small departures from the cloud characteristics. The solution discontinuity is apparent only on the volume fraction α and the droplets velocity field $\mathbf{u}$ is parallel to the contact discontinuity, as is usual for such discontinuity. Such features of the solution allow the use of the non-conservative form of the momentum equation, without compromising accuracy compared with the conservative form. Other details concern-

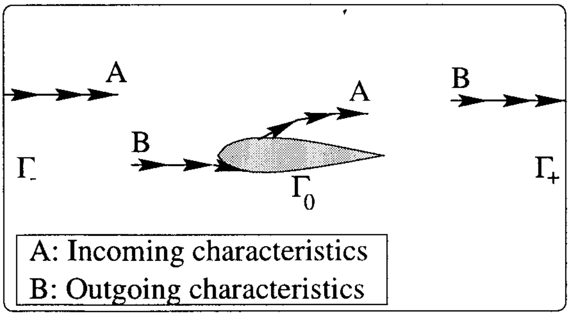

Figure 1. Computational domain.

ing the conservative form of the droplets equations can be found in Durst *et al.* [4], Hallman *et al.* [5] and Wallis [7].

3. BOUNDARY CONDITIONS AND WELL-POSEDNESS OF THE DROPLETS PROBLEM

The system (1) and (2) is easily amenable, after linearization, to a stability analysis, similar to those in Kreiss and Lorenz [8], to determine where boundary conditions are needed. Looking at the detailed analysis for Equation (2), the question is that of the choice of the boundary conditions to be imposed on **u**. The linearized Equation (2) writes as

$$\frac{\partial \mathbf{u}}{\partial t} + \mathbf{u}_0 \cdot \nabla \mathbf{u} + K_{\mathrm{D}} \mathbf{u} = \mathbf{f}, \tag{4}$$

where $\mathbf{u}_0$ is a droplets velocity not too far from the actual droplets velocity, K_{D} comes from the drag term and is assumed constant, **f** contains the drag forcing term in $\mathbf{u}_{\mathrm{a}}$ and the gravity term. After multiplication by **u**, integration over the computational domain Ω and integration by parts, one obtains

$$\frac{\partial}{\partial t} \|\mathbf{u}\|_{0,\Omega}^2 + 2K_{\mathrm{D}} \|\mathbf{u}\|_{0,\Omega}^2 = \int_{\Omega} |\mathbf{u}|^2 \operatorname{div} \mathbf{u}_0 \, \mathrm{d}x - \int_{\partial\Omega} |\mathbf{u}|^2 \mathbf{u}_0 \cdot \mathbf{n} \, \mathrm{d}s + 2 \int_{\Omega} \mathbf{f} \cdot \mathbf{u} \, \mathrm{d}x,$$

n being the outward normal to the domain boundary. The integral on $\partial\Omega$ has to be split in two parts, one on $\partial\Omega_- = \{x \in \partial\Omega\colon\ \mathbf{u} \cdot \mathbf{n} < 0\}$, which remains on the right-hand-side and one on $\partial\Omega_+ = \partial\Omega \backslash \partial\Omega_-$ which goes to the left-hand-side of the last equality and is bounded below by zero. It results in

$$\frac{\partial}{\partial t} \|\mathbf{u}\|_{0,\Omega}^2 + 2K_{\mathrm{D}} \|\mathbf{u}\|_{0,\Omega}^2 \leq \|\operatorname{div} \mathbf{u}_0\|_{\infty,\Omega} \|\mathbf{u}\|_{0,\Omega}^2 + \int_{\partial\Omega_-} |\mathbf{u}|^2 |\mathbf{u}_0 \cdot \mathbf{n}| \, \mathrm{d}s + 2\|\mathbf{f}\|_{0,\Omega} \|\mathbf{u}\|_{0,\Omega},$$

i.e. using Hölder inequality on the last term,

$$\frac{\partial}{\partial t} \|\mathbf{u}\|_{0,\Omega}^2 \leq [\|\operatorname{div} \mathbf{u}_0\|_{\infty,\Omega} + 2K_{\mathrm{D}} + 1] \|\mathbf{u}\|_{0,\Omega}^2 + \int_{\partial\Omega_-} |\mathbf{u}_\infty|^2 |\mathbf{u}_0 \cdot \mathbf{n}| \, \mathrm{d}s + \|\mathbf{f}\|_{0,\Omega}^2.$$

Here $\mathbf{u}_\infty$ stands for the boundary values of **u** on $\partial\Omega_-$. The idea is to bound the energy norm of the solution with and only with terms depending on data and parameters associated with the problem solved. An application of the Gronwall inequality ([8], p. 85) gives the ultimate energy bound:

$$\|\mathbf{u}(t)\|_{0,\Omega}^2 \leq e^{Mt} \left\{ \|\mathbf{u}(0)\|_{0,\Omega}^2 + \int_0^t \left[\int_{\partial\Omega_-} |\mathbf{u}_\infty|^2 |\mathbf{u}_0 \cdot \mathbf{n}| \, \mathrm{d}s + \|\mathbf{f}\|_{0,\Omega} \right] \mathrm{d}\tau \right\}, \tag{5}$$

where

$$M = \sup_{\tau \in [0,T]} \{ \|\operatorname{div} \mathbf{u}_0(\tau)\|_{\infty,\Omega} + 2K_{\mathrm{D}} + 1 \}. \tag{6}$$

The boundedness of the energy norm of **u** is guaranteed by the introduction of the boundary condition $\mathbf{u} = \mathbf{u}_\infty$ on $\partial\Omega_-$. Without that boundary condition, no *stability* and *unicity* would be recovered for **u**.

A similar analysis reveals that a boundary condition should be imposed on the volume fraction α on the inflow boundary $\partial\Omega_-$ as well. Hence, a boundary condition is needed on the inflow boundary for every variable and no boundary condition is needed on slip or outflow boundaries. Here, slip, inflow and outflow boundaries are defined with respect to the droplets velocity field. In other words, boundary conditions are needed on boundaries with incoming characteristics, the direction of which being controlled by the droplet velocity **u**. The inflow outer boundary, noted Γ_- (Figure 1), obviously requires boundary conditions.

The question to know whether or not the airfoil, or a part of it, presents incoming characteristics is a more subtle one. For sure, incoming characteristics are not desirable, as it would potentially mean injection of water droplets from the airfoil to the flow. Fortunately, it can be shown by integrating Equation (2) along its characteristics, that no droplet trajectory can be incoming into the computational domain from the airfoil surface. This result is true as long as the gravity force is neglected, the air flow does not slip (as with NS flow) and the droplets are initially at rest on the airfoil surface. The characteristic curve $\chi(x, t; \tau)$ passing through the point x at time t satisfies the following ODE

$$\frac{\mathrm{d}\chi}{\mathrm{d}\tau} = \mathbf{u}(\chi, \tau) \quad \text{and} \quad \chi(x, t; t) = x. \tag{7}$$

Rewriting Equation (2) using these characteristic co-ordinates, one obtains

$$\frac{\mathrm{d}\mathbf{u}}{\mathrm{d}t}(\chi, \tau) + K_{\mathrm{D}}\mathbf{u}(\chi, \tau) = K_{\mathrm{D}}\mathbf{u}_{\mathrm{a}}(\chi, \tau) \tag{8}$$

and, assuming K_{D} is constant, the solution at time t is given by

$$\mathbf{u}(\chi, t) = \mathrm{e}^{K_{\mathrm{D}}t}\mathbf{u}(x, 0) + K_{\mathrm{D}}\int_0^t \mathbf{u}_{\mathrm{a}}(\chi, \tau)\,\mathrm{d}\tau. \tag{9}$$

Equations (7) and (9) completely define a unique solution to Equation (2). Provided $\mathbf{u}(x, 0) = 0$ and $\mathbf{u}_{\mathrm{a}}(x, \tau) = 0$ (no-slip condition), for all times τ and points x on the airfoil surface, the sole solution would be $\mathbf{u} \equiv 0$ and $\chi = x$ for incoming characteristics going from the airfoil into the domain, as the information travels from upstream to downstream along the characteristic curve. Hence, the droplets can only impinge or slip on the airfoil surface, given appropriate initial conditions, and no boundary conditions are needed on the airfoil. The above analysis gives confidence to the proposed Eulerian approach to droplets impingement.

The previous result helps in the selection of an initial solution ensuring the physical meaning of the final one. One choice is to take $\mathbf{u} = (\cos(\mathrm{AOA}), \sin(\mathrm{AOA}))$ and $\alpha = 1$ everywhere except near the airfoil surface, where both variables are forced to zero. Here, AOA stands for the angle of attack of the airfoil.

4. FINITE ELEMENT FORMULATION OF THE DROPLETS MODEL

Given a triangulation of the domain Ω and the space V_h of continuous piecewise linear elements, the volume fraction on $\alpha^n \in V_h$ and the droplet velocity $\mathbf{u}^n \in V_h^2$ at time t^n are solutions of

$$\int_\Omega \left[\frac{\alpha^n - \alpha^{n-1}}{k} + \nabla \cdot (\alpha^n \mathbf{u}^n)\right]\varphi\,\mathrm{d}x + a_\alpha(\alpha^n, \varphi) = 0, \tag{10}$$

$$\int_\Omega \left[\frac{\mathbf{u}^n - \mathbf{u}^{n-1}}{k} + \mathbf{u}\cdot\nabla\mathbf{u}^n\right]\cdot\psi\,\mathrm{d}x + a_u(\mathbf{u}^n, \psi) = \int_\Omega \mathbf{f}\cdot\psi\,\mathrm{d}x \tag{11}$$

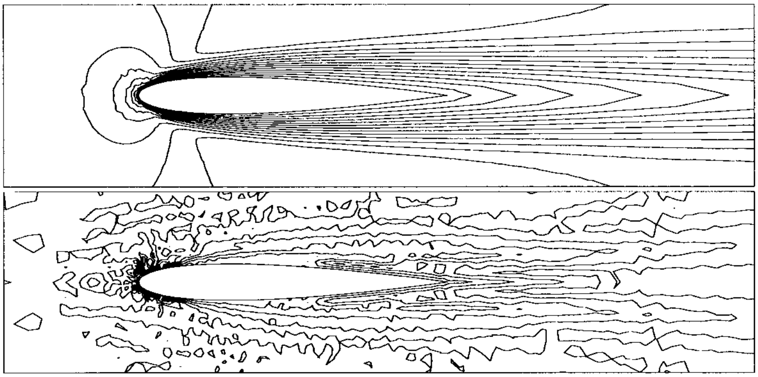

Figure 2. Numerical solution without stablization term: horizontal component of droplets velocity (top) and volume fraction of water (bottom); air speed = 156 m s^{-1}, AOA = 0°, MVD = 20 µm, LWC = 1 g m^{-3}).

for all $\varphi \in V_h$, $\psi \in V_h^2$ such that $\varphi, \psi = 0$ on Γ_-. Here, **f** stands for the drag and gravity forces on the droplets, thus depending on **u** and $\mathbf{u}_a$; k is the time step used for calculating steady and unsteady solutions, as pseudo time stepping is used in the former case. The extra terms $a_\alpha(\cdot,\cdot)$ and $a_u(\cdot,\cdot)$ are stabilization terms to be defined below.

The following boundary conditions are imposed node by node on Γ_-:

$$\alpha^n = 1 \quad \text{and} \quad \mathbf{u}^n = (\cos(\text{AOA}), \sin(\text{AOA})). \tag{12}$$

While the finite element method (FEM) has been presented for the non-conservative form of (1) and (2), it is not difficult to write down the scheme for the conservative form.

Stabilization terms are added to remove possible oscillations in the droplets solution. This could, for example, be a classical artificial viscosity or a streamline upwinding (SUPG) term [9]. These stabilization terms are of the form

$$a_\alpha(\alpha, \varphi) = c_\alpha \sum_K h_K \int_K |\mathbf{u}^{n-1}| \nabla \alpha^n \cdot \nabla \varphi \, \mathrm{d}x, \tag{13}$$

$$a_u(\mathbf{u}, \psi) = c_u \sum_K h_K \int_K |\mathbf{u}^{n-1}| \nabla \mathbf{u}^n \cdot \nabla \psi \, \mathrm{d}x \tag{14}$$

for the classical artificial viscosity case, and

$$a_\alpha(\alpha, \varphi) = c_\alpha \sum_K \int_K \left[\frac{\alpha^n - \alpha^{n-1}}{k} + \nabla \cdot (\alpha^n \mathbf{u}^n) \right] \tau_K (\mathbf{u}^n \cdot \nabla) \varphi \, \mathrm{d}x, \tag{15}$$

$$a_u(\mathbf{u}, \psi) = c_u \sum_K \int_K \left[\frac{\mathbf{u}^n - \mathbf{u}^{n-1}}{k} + \mathbf{u}^n \cdot \nabla \mathbf{u}^n - \mathbf{f} \right] \cdot \tau_K (\mathbf{u}^n \cdot \nabla) \psi \, \mathrm{d}x \tag{16}$$

for the SUPG case. τ_K is equal to $h_K / \sqrt{1 + |\mathbf{u}|^2}$, h_K being the minimal size of the element K, c_α and c_u are parameters chosen by the user.

It is mainly the volume fraction that requires some extra stabilization, as the velocity suffers little numerical instabilities (Figure 2). It was suspected, at first observation, checkerboard instabilities like those observed on the pressure with unstable finite elements for incompressible flows [10]. A mixed method, using a quadratic element for the droplet velocity and a linear one for the volume fraction, was implemented and tested. Oscillations were still observed on the volume fraction, suggesting that the instabilities are mainly due to the non-linear convective terms. Figure 3 shows the improvement on the volume fraction obtained with the classical artificial viscosity and the SUPG terms. The SUPG term seems to be a little more efficient, although the differences observed probably come from the tuning of the parameters c_α and c_u. In that respect, the SUPG method is much less sensitive to the tuning of the parameters.

A Newton–GMRES matrix-free algorithm was used to solve the droplets system of equations. At each iteration of the Newton method, the linear system involving the Jacobian matrix of the non-linear system is solved with the GMRES method. The Jacobian matrix appears only in matrix–vector products, these latter being approximated using a finite difference formula on the residuals. The computations and storage of the Jacobian matrix are then avoided, at the expense that more residuals have to be evaluated at each time step. Generally speaking, the technique has less time step restriction than an explicit method with a low memory requirement, sufficiently low to be usable on a good workstation in 3D. See Brown and Saad [11] for a complete description of the Newton–GMRES algorithm with a finite difference approximation of matrix–vector products.

As far as the appropriate way to write the droplets system is concerned, no obvious difference was observed between the solutions obtained with the conservative and non-conservative forms of the equations, except for lower computing times using the non-conservative form. Hence, the FEM based on the non-conservative form of (1) and (2) of the droplets equations and on the SUPG stabilization term is preferred, in terms of computing time, simplicity of coding and quality of the numerical solutions.

5. DETERMINING COLLECTION EFFICIENCY

An important parameter that controls the accretion of ice on an airfoil is the local collection efficiency β, i.e. the normalized flux of water on the aerodynamic surface. To compute the collection efficiency with the Lagrangian particle tracking, one must determine if a droplet impacts the airfoil or not along its trajectory, compute the impact point for droplets within the impingement limit, which is not known in advance, and then evaluate the distance between neighboring droplets. This strategy becomes cumbersome to implement for multi-element airfoils [12] and even more so in 3D [2].

Within the Eulerian approach, the collection efficiency is computed on every edge (face in 3D) belonging to the aerodynamic surface using

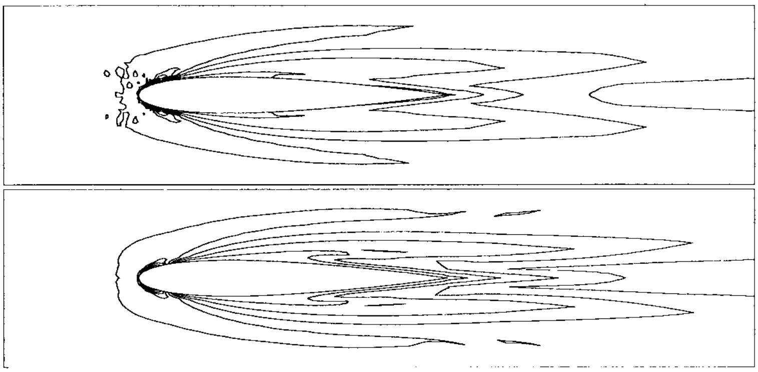

Figure 3. Volume fraction of water with stabilization term: classical artificial vicosity (top) and SUPG (bottom); air speed = 165 m s^{-1}, AOA = 0°, MVD = 20 μm, LWC = 1 g m^{-3}).

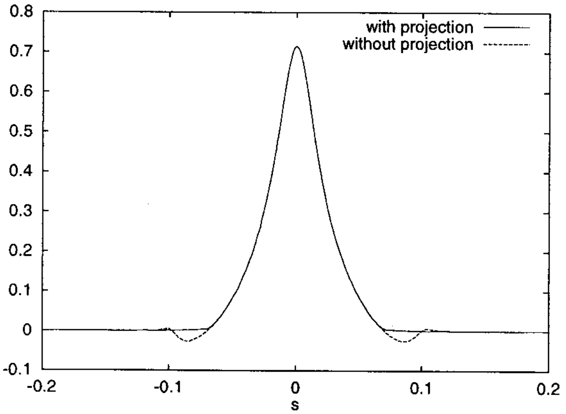

Figure 4. Local collection efficiencies β as a function of the arc length s (in inches) of the airfoil as obtained with and without projection of the droplets velocity (AOA = 0°).

$$\beta = \alpha \mathbf{u} \cdot \mathbf{n},$$

The water flux m_{w} at the airfoil surface would then be

$$m_{\mathrm{w}} = \mathrm{LWC}\ U_{\infty}\beta.$$

Some special attention is required for the computation of the normal **n** to the airfoil surface, but apart from that, the recovery of the collection efficiency can be coded very simply and the code would handle multi-element airfoils the same way as single element ones. Actually, the normal **n** and the collection efficiency β are computed at the center of every edge on the airfoil. It should be noted that the presence of one or another stabilization term, even of none at all, has almost no effect on the collection efficiencies recovered.

It has been proven in Section 3 that no incoming characteristics exist on the airfoil for the solution of the continuous problem with the boundary and initial conditions proposed. The exclusion of incoming characteristics contains in itself a monotonicity condition, i.e. the normal component of the droplets velocity must be positive on the airfoil. But, in the discrete case, the actual finite element method cannot guarantee naturally that this monotonicity condition on the normal velocity is satisfied. For example, Figure 4 shows the effect of that loss of monotonicity on the local collection efficiency. While going from the stagnation point to the impingement limits, the droplets velocity gradually becomes parallel to the airfoil surface. Hence, the normal component of the droplets velocity approaches zero near the impingement limits and the numerical method has growing difficulties ensuring its positivity in these areas. This behavior is not atypical as the same difficulty may occur with the positivity of the density or the pressure while computing compressible flows with many numerical methods.

Although the refinement of the mesh near the impingement limits reduces the strength of the undershoot on the local collection efficiency, it is preferable to use the same mesh for air and droplets computations and correct the loss of monotonicity of the normal component by an appropriate projection along the airfoil. The normal components of the droplets velocity can be computed at the two vertices of an element edge on the airfoil and set to zero provided these normal components are negative. Then, proceed to the following edge on the airfoil. Although this type of projection is dependent on the order of the edges in the list of airfoil edges, it avoids the definition of a normal to the airfoil at the edge vertices, in itself a nightmare especially near sharp corners. Moreover, the application of the projection is limited to a very small area on the airfoil, only slightly modifying the droplets velocity and having negligible effect as grids get refined. A comparison of the collection efficiency with and without projection is made in Figure 4.

The computation of flows with droplets of different sizes can be done by splitting the diameters distribution in a finite number of classes and by solving independently one droplets' system for each class. If the percentage of droplets in the ith class is given by p_i, the overall collection efficiency would be

$$\beta = \sum_i p_i \beta_i$$

for β_i, the ith class collection efficiency. Hence, the droplets code does not have to be modified to handle polydispersed droplets, as long as the change of air momentum due to droplets is neglected.

6. FLOW FIELD COMPUTATIONS AND MESH ADAPTATION TECHNIQUES

A complete characterization of airfoil performance must account for the viscous forces, if both lift and drag are to be recovered. The resolution of the full compressible Navier–Stokes equations, combined with appropriate turbulence models, is the most promising avenue for such performance assessment. Internal and external flows could then be computed with the same code, providing the opportunity for aircraft and engine designers to integrate their efforts in simulating performance degradation due to ice. Moreover, by solving the Navier–Stokes equations, heat transfer would then be computed in a natural and almost automatic way, even in complex icing situations. This last feature is of major importance for the simulation of ice accretion, de- and anti-icing heat transfer, as well as for the optimal design of anti-icing devices.

Among the technologies available today for the solution of the Navier–Stokes equations, the FEM is one of the most versatile. This numerical method can be applied in a multi-disciplinary way to the equations of fluids and of structures, for arbitrary geometries. For example, once a finite element Navier–Stokes solver has been coded, it can be easily used on single and multi-element airfoils, without modifications.

In the present study, different FE solvers were used, as needed and as available, to compute the air flow. The flow field solvers were kept independent of the droplet solver, simply to allow more flexibility in the choice of these solvers. Numerous computations were carried out using a NS solver on triangular meshes [13,14], but also using Euler solvers on quadrilateral [15] and triangular [16] meshes.

The choice of one or other flow FE solver is proved not to be that critical, as a very efficient remesher was used to obtain an adapted mesh over which a mesh-independent and solver-independent solution of the Euler or NS equations can be computed [17]. Here, *mesh-independence* is to be understood as the independence of the final mesh and solution from the mesh used to initiate the adaptation process. Otherwise, the accuracy of any numerical solution is highly dependent upon the mesh used, not only in terms of the size of the elements but also with respect to their orientation and aspect ratio. Directional flow structures, such as shock waves and boundary layers, ask for *anisotropic* elements. The second derivative of the local Mach number is then used to control the amplitude and the direction of the numerical solution error, hence the size and the orientation of the elements, over the mesh. The present adaptation library computes iteratively a mesh adapted to the test case, starting with a generic mesh.

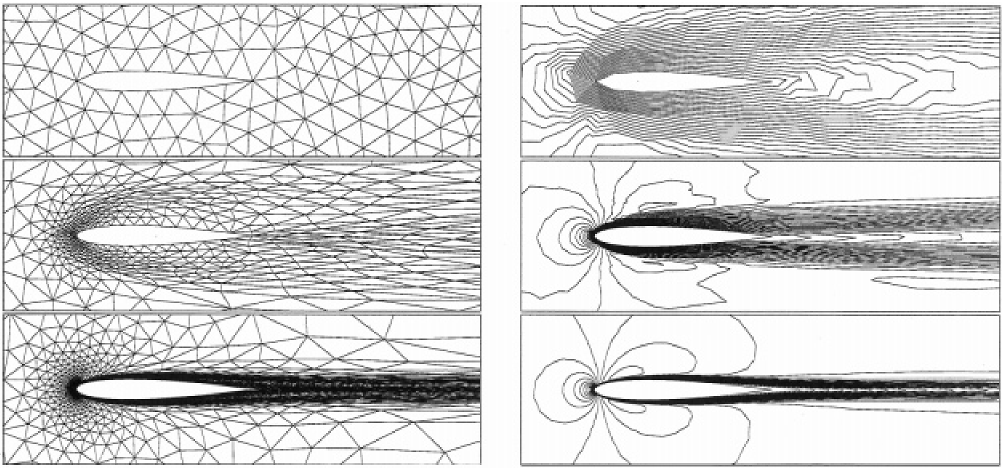

Figure 5. Initial mesh and solution (top), second adapted mesh and solution (middle) and final adapted mesh and solution (bottom) for a viscous flow at $Ma = 0.236$, $Re = 8000$, AOA = 0°.

To illustrate the evolution of the mesh during the solver/remesher iterations, Figure 5 shows the initial, second and final meshes and solutions (Mach contours) for a subsonic flow over a NACA0012 airfoil. One should note how close the solutions fit the meshes. The adaptative process is convergent, as can be seen in Figure 6. While improving the mesh at each adaptation step, the C_f curves get closer and closer to the final one. The friction coefficient $C_f = \tau_{wall}/(0.5\rho_\infty U_\infty^2)$ is plotted, as usual, against the non-dimensional co-ordinate x/C with τ_{wall} the viscous stress along the wall and C the chord length of the airfoil.

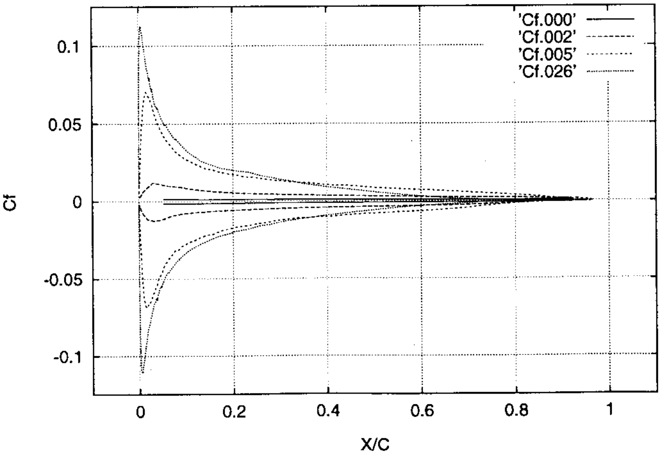

Figure 6. Evolution of the C_f curves with the solver–remesher iterations for a viscous flow at $Ma = 0.236$, $Re = 8000$, AOA = 0° (# in legend indicates adaptation iteration).

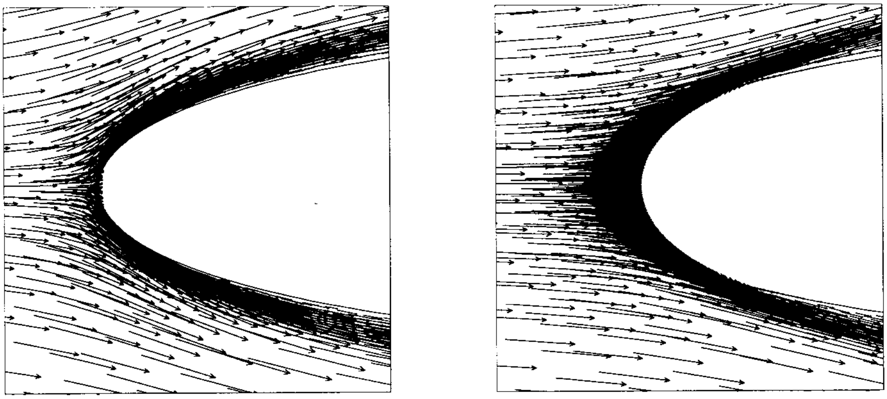

Figure 7. Air velocity (left) and water droplets velocity (right); $Ma = 0.236$, $Re = 8000$, AOA = 0°, MVD = 16 μm, LWC = 1 g m^{-3}.

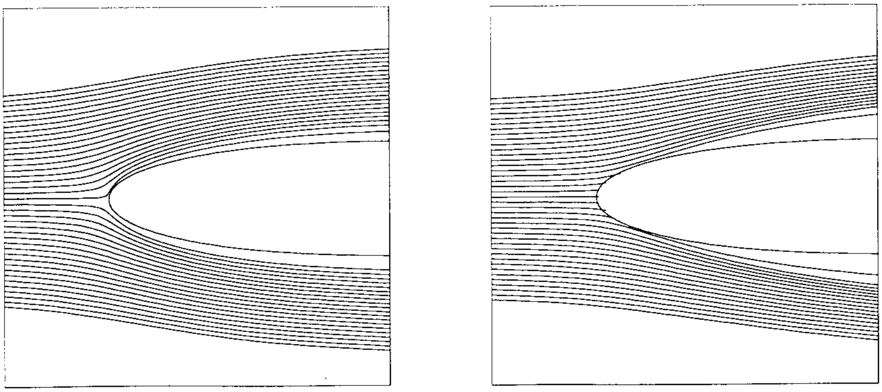

Figure 8. Streamlines (left) and droplets trajectories (right) for velocity fields of Figure 7.

7. RESULTS AND COMPARISONS

Numerical results for droplets impingement on a NACA0012 single element airfoil are first presented. Comparisons with experiments, based on a NASA series of icing tunnel tests [1] are also reported. Computations using a Langmuir distribution of droplet sizes are shown to improve the accuracy of the collection efficiency near the impingement limits. Next, numerical results on a multi-element NASA airfoil are given. In particular, the sensitivity of the droplets solution and collection efficiency on the characteristics of the flow, inviscid or viscous, is illustrated by the results. Finally, the variation of the collection efficiency as a function of the MVD is considered on the NACA0012 and the multi-element airfoil.

7.1. NACA0012 airfoil, single droplets size

A typical output of the Eulerian droplet code is the volume fraction, as in Figure 3, and the droplets velocity field, as in Figure 7. In the latter figure, a clear difference is observed on the leading edge where the air stops on the airfoil surface, while the droplets hit the surface with a strictly positive speed. Here, the air speed is 80 m s^{-1} ($Ma = 0.236$), the angle of attack 0°, the droplet mean volume diameter 16 μm and the LWC is equal to 1 g m^{-3}. For test cases such as this one, where the flow is steady, the flow solver is run until some convergence is reached and then, the droplets solver is started using the initial solution presented above. The droplets time marching computations are carried long enough to ensure that a steady state is reached near the impingement area. As a result, these computations may be stopped before the complete wash out of the droplets in the wake of the airfoil. But this has no effect on the accuracy of the collection efficiency computed.

A Lagrangian particle tracking code usually computes droplets trajectories and uses them to calculate the collection efficiency. With an Eulerian code, even if the trajectories are not needed for computing the collection efficiency, they still can be recovered, in the steady case, by plotting the streamlines of the droplets velocity field with any flow visualization package. The trajectories shown in Figure 8 have been computed in that manner, using the droplets velocity field of Figure 7. Some droplets trajectories hit the leading edge due to the inertia of the droplets, while the flow streamlines avoid the airfoil (except the one ending at the stagnation point). In that respect, massless droplets would follow the flow exactly and act as flow markers.

In Figure 9, the collection efficiencies for the test case of Figure 3 are plotted against the arc length s of the airfoil. The technique for collection efficiency recovery explained above has

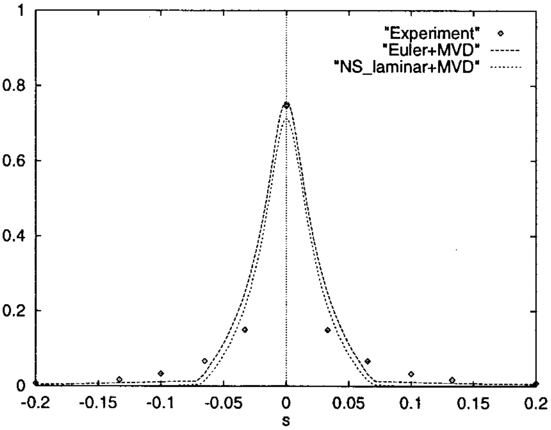

Figure 9. Local collection efficiency β as a function of the arc length s (in inches) of the airfoil (AOA = 0°).

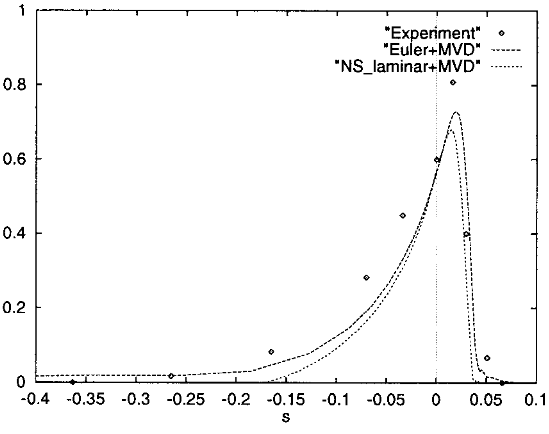

Figure 10. Local collection efficiency β as a function of the arc length s (in inches) of the airfoil (AOA = 8°).

Table I. Langmuir D distribution of droplet diameters for a MVD of 16 μm

Percentage LWC (%)	Ratio of diameters	Droplet diameter (μm)
0.05	0.31	5.0
0.10	0.52	8.3
0.20	0.71	11.4
0.30	1.00	16.0
0.20	1.37	21.9
0.10	1.74	27.8
0.05	2.22	35.5

been used. Two numerical results are shown, one combines an Euler flow computation with a droplets solution, the other a laminar Navier–Stokes solution at $Re = 8000$, again with an Eulerian droplets computation. The agreement with experimental results is quite good in both cases. The gap between the collection efficiency curve for the Navier–Stokes flow and the one for the Euler flow is thought to be due to the large thickness of the boundary layer in the laminar regime. A turbulent Navier–Stokes solution at the experimental Reynolds number of 1.6×10^6 would probably reduce the gap between the two curves and is the next step in the authors' research. It is also expected that an inviscid flow simulation does well for this test case, simply because the turbulence intensity in the leading edge impingement area is quite low.

The results for a second test case with an angle of attack (air speed = 80 m s^{-1}, AOA = 8°, MVD = 16 μm, LWC = 1 g m^{-3}) are shown in Figure 10. The agreement between experimental and numerical results is quite good. Again the boundary layer thickness for the laminar NS flow ($Re = 8000$) should account for the reduced local collection efficiency when compared with the inviscid Euler flow. Note that for this particular test case, the experimental repeatability of the collection efficiency may not be as good as in the 0° AOA and could explain the larger gap between computed and experimental results.

7.2. NACA0012, Langmuir distribution of droplet sizes

Droplets clouds, however, usually present themselves with a distribution of droplet diameters instead of droplets of the same size. The Langmuir D distribution, as given in Table I for

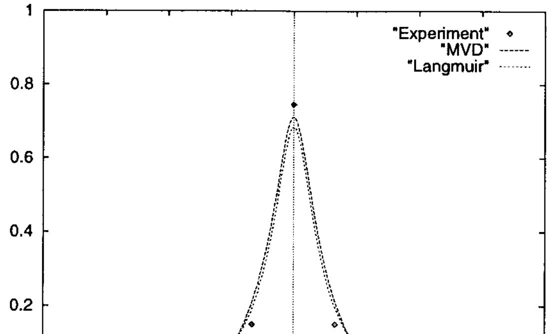

Figure 11. Local collection efficiency β for MVD droplets or a Langmuir D distribution of droplets (AOA = 0°).

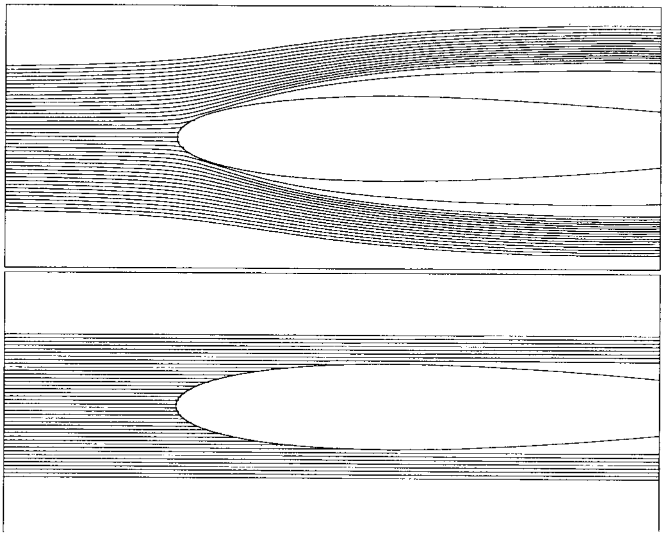

Figure 12. Droplets trajectories for two MVD, 20 μm (top) and 1000 μm (bottom); $Ma = 0.236$, $Re = 8000$, AOA = 0°.

a MVD of 16 μm, is a typical one for an icing cloud [1,18]. Figure 11 compares the collection efficiency for monodispersed droplets of MVD and for polydispersed droplets with a Langmuir D distribution of diameters. Impingement limits are more accurately predicted with polydispersed droplets. The maximum value of the collection efficiency is larger for the monodispersed droplets. The droplets computations can be carried independently for each droplets class or one can use the solution of the previous droplets class to reduce the computing time of the next class solution. In both cases, the cumulative collection efficiency is recovered after all droplets solutions have been obtained.

7.3. Supercooled large droplets

The current trend of the in-flight icing research is to emphasize supercooled large droplets (SLD). The certification process for aircraft may have to be modified to account for distributions of droplets with a MVD well above the maximal 40 μm used now. For freezing drizzle, the MVD is around 200 μm and for freezing rain it can reach 1000 μm. For such large droplets, the 1% fluctuation control volume introduced above for 20 μm droplets clearly has to be enlarged. Otherwise, the volume fraction and the Eulerian droplets velocity have to be understood as averages with a higher fluctuation percentage if the control volume is kept fixed while going from 20 μm droplets to SLD. But dealing with averages instead of fluctuating quantities is more in the spirit of engineering practice (as in turbulence modeling). Even in the Lagrangian context, all the droplets computations done so far for icing simulations had the objective of predicting average collection efficiencies. Tracking individual droplets is unaffordable on actual computers. There are over 1000 droplets for a MVD of 20 μm in a cubic box of the order of 1 cm^3. Hence, each droplet tracked by the Lagrangian code represents a set of real physical droplets nearby. In that respect, the Eulerian approach stands closer to the final objective of predicting averages. Keeping in mind that fluctuation around the average may be more important for larger MVD, this latter approach makes sense for large droplets as well.

The validity of the assumptions behind the Eulerian model could be questioned for SLD, in particular the first two hypotheses given in Section 2. Some insight on the validity of the spherical droplets and no break-up assumptions could be gained by looking at Cheremisinoff [19] and references therein. It is generally agreed that droplets up to 1 mm diameter remain nearly spherical, but that larger drops deviate from spherical shapes, by first oscillating around a spherical equilibrium shape. One of the parameters that controls droplet break-up in free air is the Weber number, whose value should be above 10–20 for water droplets break-up. For the SLD solutions shown here, the Weber number reaches the critical values in a very narrow area close to the airfoils; so close in fact that it is probably too late for the droplets break-up to have an impact on the collection efficiency. As for the second assumption, SLD conditions are generally associated with smaller LWC with even less frequent collision and coalescence phenomena. Splashing occurs when the droplets impact on the wall, eventually requiring a new way to recover the collection efficiency or at least a reinterpretation of the collection efficiency actually computed. Modification of the droplets PDEs would be needed for a detailed analysis using SLD size distributions, where small droplets should be reinjected in the flow close to the wall due to splashed droplets break-up. The present analysis only considers MVD for SLD.

As large droplets have more inertia, it is expected that their trajectories get closer and closer to straight lines. The results of Figure 12 agree qualitatively with this remark. The 20 μm droplets trajectories recovered at post-processing are clearly curved, while the 1000 μm ones appear as straight lines for the given flow conditions. The convergence of the trajectories to straight lines when the droplets size increases results in the convergence of the collection efficiency predicted using the MVD to a limit one. On Figure 13, this may be seen by comparing the small gap between the 200 and 1000 μm β curves with the large gap between the 20 and 200 μm ones. This last conclusion applies directly to the variation of the impingement limits while increasing the MVD. As a consequence, the shift from the classical *FAR-25 Appendix C* less than 40 μm droplets should require a deeper revision of assumptions and designs than the shift from freezing drizzle to freezing rain.

7.4. Multi-element airfoil

Numerical results are presented for a four-element airfoil taken from Omar *et al.* [20], whose leading edge slat is at 45°, the first trailing flap at 25° and the second flap at 51.2°. The cloud's

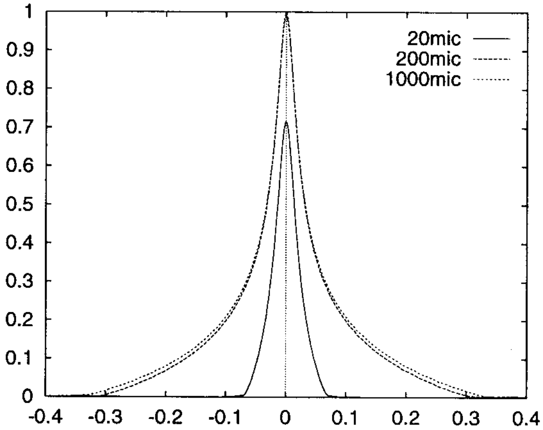

Figure 13. Variation of the collection efficiency β with the MVD.

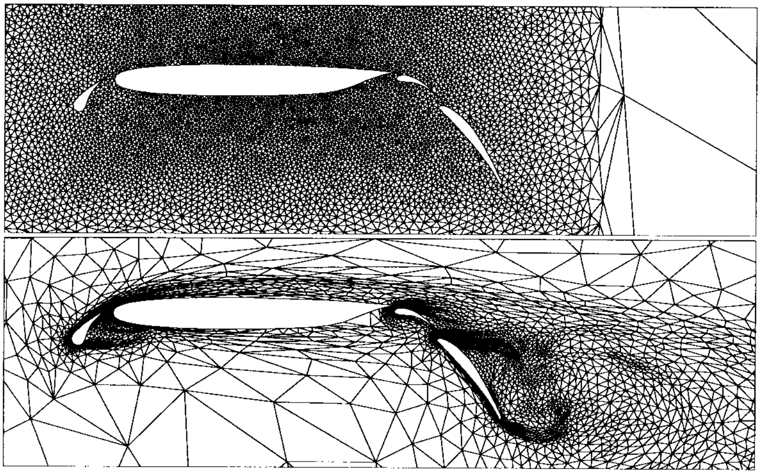

Figure 14. Initial mesh (top) and adapted mesh (bottom) for a four element airfoil.

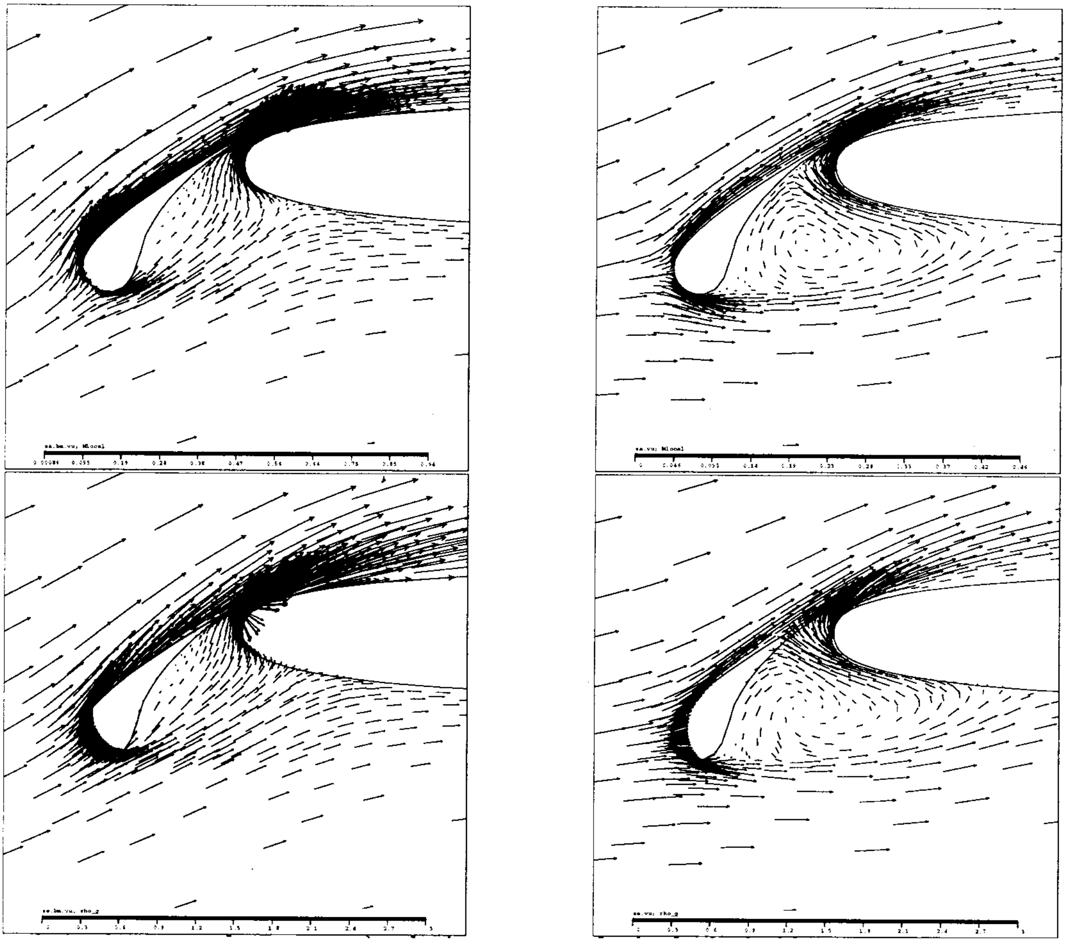

Figure 15. Air (top) and droplets (bottom) velocity over the slat in the inviscid case (left) and the viscous case $Re = 5000$ (right); $Ma = 0.3$, AOA = 0°, MVD = 20 μm, LWC = 1.05 g m^{-3}.

droplets diameter is 20 μm and the air velocity 94 m s^{-1}, with a 0° angle of attack. The initial mesh and the final one given by the adaptative library are shown in Figure 14. The final mesh has been adapted to the air flow but is also used for the droplets computations. As can be seen on this figure, not much effort has been put on the initial mesh, the adaptative library improving it remarkably.

Multi-element airfoils are typical configurations where viscous effects have a strong impact on the flow. For example, Figure 15 shows the huge difference between an inviscid flow and a laminar viscous one at $Re = 5000$. An unsteady vortex appears besides the slat in the viscous case. An impact of the viscous forces in this particular example is the upward displacement of the stagnation point when compared with the inviscid one. The displacement of the stagnation point clearly has an effect on the position of the impingement area on the slat, as can be seen in Figure 15. Similar differences between the inviscid and viscous flows have been observed on the flaps and the main element. These remarks are confirmed by Figure 16, where the local collection efficiency β is plotted along each element of the airfoil in the outward normal direction. Of course, all these results on droplets impingement with laminar flows have to be further confirmed for turbulent ones.

The following comments have to be made concerning the computing strategy for the viscous flow multi-element airfoil example. Provided the air flow is steady, one can freeze the air variables and let the droplets' solver reach a steady state. An example of this situation over the multi-element airfoil is provided by the inviscid flow presented above. For unsteady air flows with moving vortices, however, a stronger coupling of the air and droplets solver is needed. Using the strategy for steady flows in this latter case, the frozen vortices would centrifuge the droplets, creating an endless accumulation of water at the periphery of these vortices. To prevent this type of divergent behavior, one should alternate between the air and droplets solvers in order to move the vortices and prevent the overaccumulation of water.

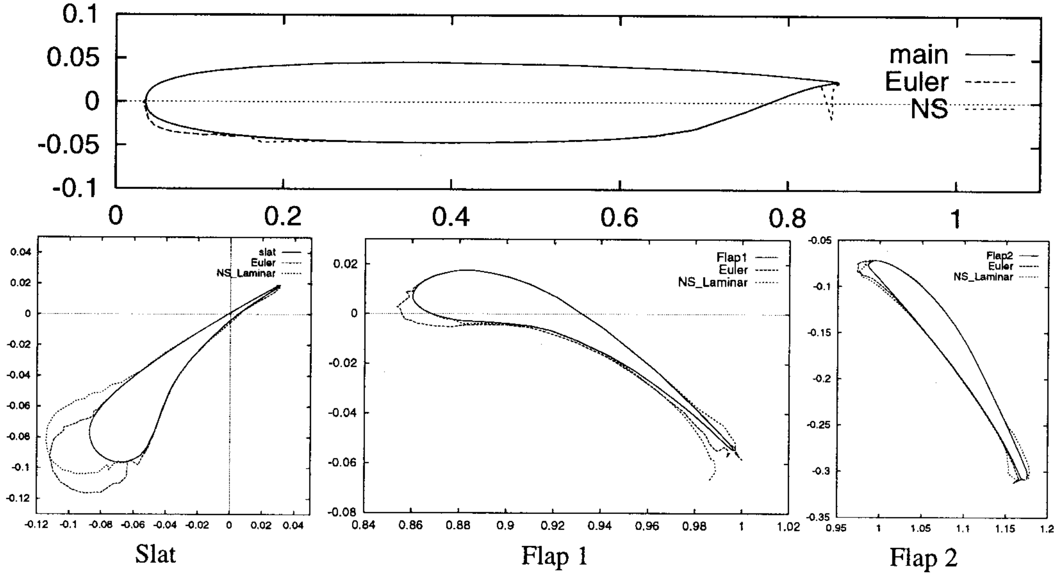

Slat Flap 1 Flap 2

Figure 16. Local collection efficiency β plotted along each element of the multi-element airfoil for viscous and inviscid flows (β plotted normal to the surface).

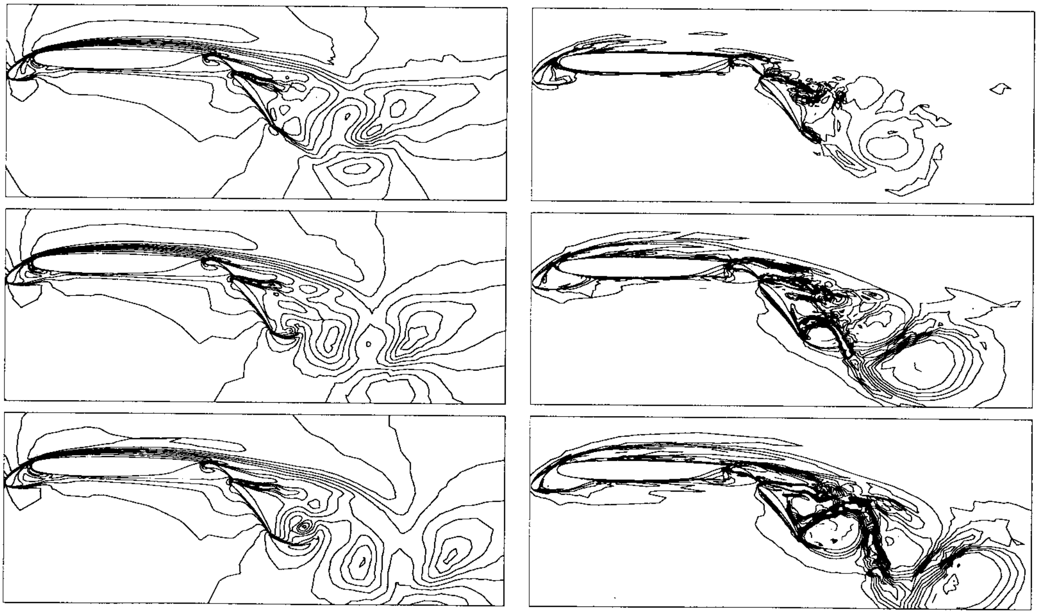

Figure 17. Time evolution of the Mach contours for the air (left) and of the droplets volume fraction (right) for an unsteady viscous flow over a multi-element airfoil; $Ma = 0.3$, $Re = 5000$, AOA = 0°, MVD = 20 μm, LWC = 1.05 g m^{-3}.

The time evolution of the air and droplets solutions is illustrated in Figure 17, starting with an established air solution and a uniform droplets solution. As with the NACA0012 airfoil, the droplets solution establishes itself rapidly on the exposed surfaces of the slat and the flaps. The

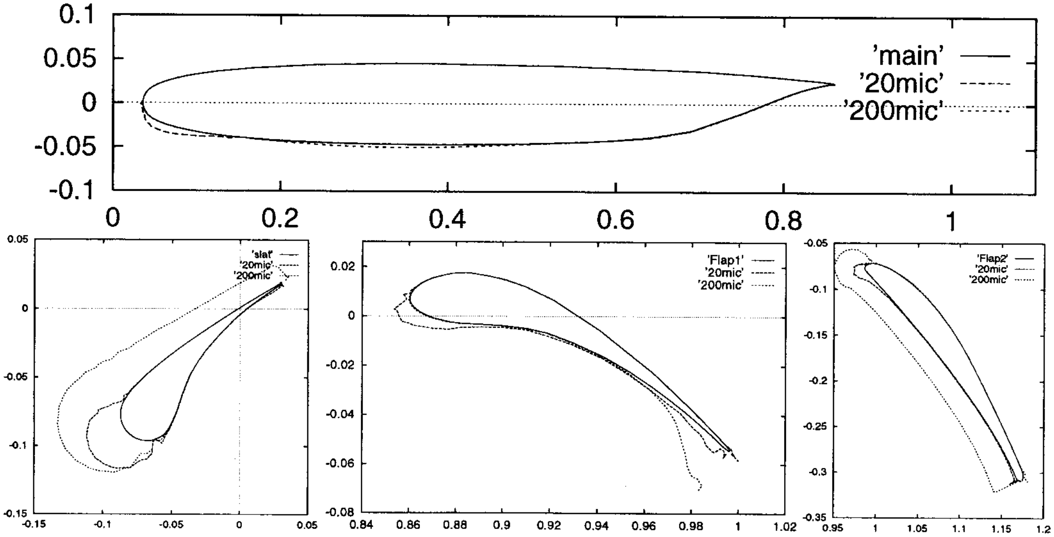

Slat Flap 1 Flap 2

Figure 18. Local collection efficiency β plotted along each element of the multi-element airfoil for two MVD, 20 and 200 μm.

evolution of the solution on the main element takes more time, as one part of the main element stands close to the vortex behind the slat. Figure 17 also shows that the effect of the vortex shedding on the evolution of the droplets solution is taken into account by the weak coupling proposed. Hence, the actual Eulerian methodology appears as a promising tool for the prediction of droplets or particles impingement on components located in the wake of other ones.

As stressed above, a larger MVD results in a modification of the collection efficiency and the impingement limits. Figure 18 thus shows the local collection efficiencies plotted in the outward normal direction along all elements of the multi-component airfoil for two different MVDs. In both cases, the inviscid flow presented above served as the driving flow for the droplets computations. The variation of impingement limits and collection efficiencies is important on any element of the airfoil and cannot be guessed as easily as for the NACA0012 airfoil.

8. CONCLUSION

The Eulerian approach proposed for the computation of droplets impingement has been shown to be feasible, efficient and accurate. By itself, the Eulerian droplets model has been used several times in the past but, to the authors knowledge, never as a means to predict droplets impingement using in particular the most up-to-date computational fluid dynamics methods. Some theoretical justification of this particular use of the Eulerian approach has been given by an appropriate analysis of the boundary conditions. An implicit finite element method has been proposed, together with appropriate stabilization techniques and a non-linear iterative solver that considerably reduces the requirement for memory storage. A comparison of experimental and numerical results prove the efficiency of the method, at least in terms of accuracy and validity of the method. Of course, an extensive validation is needed, especially for more complex geometries, such as multi-element airfoils, as experimental data on such geometries becomes more available or even accessible. Moreover, a comparison of Lagrangian versus Eulerian droplets impingement calculations, using simple-to-complex test cases, is still needed to determine which method is the most computationally efficient and in what situations, as variation may be expected from test case to test case.

The generality and the simplicity of the method makes it a promising tool for computing impingement on 3D aircraft components and on engines. In fact, the implementation of a 3D droplets Eulerian code, DROP3D, is well under way. Another direction of improvement would be the use of a more sophisticated droplets collection model on the airfoil, one that could account for the size of the droplets and droplets splashing.

The unsteady droplets solution computed on the multi-element airfoil opens up avenues for a broader use of the present Eulerian method. Even if only one-way coupling has been considered, one can think about any application where an unsteady flow drives the spreading of droplets, e.g. sprays in combustion. The limitation on the smallness of the particle loading for the one-way coupling to be valid could be removed by adding a momentum exchange term in the Navier–Stokes or Euler equations. The same finite element technology would then allow the computation of unsteady particle laden gas flow in a fully two-way coupled manner.

ACKNOWLEDGMENTS

The authors acknowledge the financial support of NSERC (Natural Sciences and Engineering Research Counsil of Canada) under a Strategic Grant for the development of FENSAP-ICE (Finite Element Navier–Stokes Analysis Package), the Ministère de l'Education Supérieure du Quebec for its support under a Quebec–US Collaboration Grant and the CRM (Centre de Recherches Mathématiques) for its partial support of Julien Dompierre through a Post Doctoral Fellowship at the CFD Laboratory.

REFERENCES

1. G. Ruff and B. Berkowitz, 'Users' manual for the NASA Lewis ice accretion prediction code (LEWICE)', *Tech. Rep. 185129*, NASA, 1990.
2. T. Hedde, 'Modélisation tridimensionnelle des dépôts de givre sur les voilures d'aéronefs', *Ph.D. Thesis*, Université Blaise Pascal, 1992.
3. C. Crowe, 'Review—numerical models for dilute gas-particle flows', *Trans. ASME J. Fluids Eng.*, **104**, 297–303 (1982).
4. F. Durst, D. Milojevic and B. Schonung, 'Eulerian and Lagrangian predictions of particulate two-phase flows: A numerical study', *Appl. Math. Model.*, **8**, 101–115 (1984).
5. M. Hallman, M. Scheurlen and S. Wittig, 'Computation of turbulent evaporating sprays: Eulerian versus Lagrangian approach', *J. Eng. Gas Turbines Power*, **117**, 112–119 (1995).
6. J. Scott, W. Hankey, F. Giessler and T. Gielda, 'Navier–Stokes solution to the flow field over ice accretion shapes', *J. Aircraft*, **25**, 710–716 (1988).
7. G. Wallis, *One-Dimensional Two-Phase Flow*, McGraw-Hill, New York, 1969.
8. H. Kreiss and J. Lorenz, *Initial-Boundary Value Problems and the Navier–Stokes Equations*, Academic Press, New York, 1989.
9. T. Hughes and M. Mallet, 'A new finite element formulation for computational fluid dynamics: III The generalized streamline operator for multi-dimensional advective–diffusive systems', *Comput. Methods Appl. Mech. Eng.*, **58**, 305–328 (1986).
10. F. Brezzi and M. Fortin, *Mixed and Hybrid Finite Element Methods*, Springer Series in Computational Mathematics, Springer, Berlin, 1991.
11. P. Brown and Y. Saad, 'Hybrid Krylov methods for non-linear systems of equations', *Tech. Rep. UCRL-97645*, Lawrence Livermore National Laboratory, November 1987.
12. W. Wright and C. Bidwell, 'Additional improvements to the NASA Lewis ice accretion code LEWICE', *AIAA Paper 95-0752*, January 1995.
13. S. Boivin and M. Fortin, 'A new artificial viscosity method for compressible viscous flow simulations by FEM', *Comp. Fluid Dyn.*, **1**, 25–41 (1993).
14. Y. Bourgault, 'Méthode d'éléments finis en mécanique des fluides, conservation et autres propriétés', *Ph.D. Thesis*, Université Laval, Québec, 1996.
15. G. Baruzzi, 'A second-order finite element method for the solution of the transonic Euler and Navier–Stokes equations', *Ph.D. Thesis*, Concordia University, Montreal, 1995.
16. B. Mohammadi, 'Fluid dynamics computation with NSC2KE: A user-guide release 1.0', *Tech. Rep. RT-0164*, INRIA, 1994.
17. M.-G. Vallet, J. Dompierre, Y. Bourgault, M. Fortin and W. Habashi, 'Coupling flow solvers and grid through an edge-based adaptive grid method', *ASME Fluids Engineering Conference*, San Diego, CA, July 1996.
18. I. Langmuir and K. Blodgett, 'A mathematical investigation of water droplet trajectories', *Tech. Rep. 5418*, US Army Air Forces, 1946.
19. N.P. Cheremisinoff (ed.), *Encyclopedia of Fluid Mechanics*, vol. 3, Gulf Publishing, 1986, chap. 11.
20. E. Omar, T. Zierten, M. Hahn, E. Szpiro and A. Mahal, 'Two-dimensional wind tunnel test of a NASA supercritical airfoil with various high-lift systems', *Tech. Rep. CR-2215*, **2**, NASA, 1973.